Fabrication and magnetic properties of Sol-Gel derived NiZn ferrite thin films for microwave applications

Shauna Robbennolt[1], Stephen S. Sasaki[1], Tylisia Wallace[1], Marquise Bartholomew[1], Sarah H. Tolbert[*1,2]

[1]Department of Chemistry and Biochemistry, University of California, Los Angeles, California 90095-1569, United States.
[2]Department of Materials Science & Engineering and the California Nano Systems Institute, University of California, Los Angeles, California 90095, United States.

[*]Corresponding author

DOI: 10.5185/amlett.2018.1996
www.vbripress.com/aml

Abstract

We present a new solution-phase, sol-gel based spin-coating method to fabricating high quality, nickel zinc ferrite (NZFO) thin films. The effect of annealing temperature on the microstructure, static magnetic properties and X-band FMR linewidth and resonance field was investigated. Furthermore, the effect of composition on these properties was explored in films with the formula $Ni_xZn_{(1-x)}Fe_2O_4$ (where x = 0 to 1 in 0.1 increments). Films annealed at the highest annealing temperature of 1100 ˚C were found to have the highest saturation magnetization and coercivity, as well as the lowest FMR linewidths. Films with the composition $Ni_{0.3}Zn_{0.7}Fe_2O_4$ were found to have the lowest linewidths along with favorable magnetic properties for microwave applications. The champion film showed an FMR linewidth of 93 G, corresponding to a low Gilbert damping coefficient of $\alpha = 0.003$, a saturation magnetization of 330 emu/cm^3, and a coercivity and anisotropy field of 14 and 62 Oe respectively.

Keywords: Nickel zinc ferrite, thin film, sol-gel, FMR.

Introduction

Soft ferrites are widely used in microwave applications such as phase shifters, circulators and isolators, largely due to their high electrical resistivity and low losses at high frequencies.[1-11] Currently, most of these applications use bulk-processed ferrite powders. However, there is a significant push towards miniaturized and fully integrated microwave devices, which requires that routes to high quality, thin films of these materials be developed.[2, 3, 6, 7, 12] Soft ferrites can be divided into three classes based on their structure: garnets, hexaferrites and spinel ferrites. The most commonly used garnet is yttrium iron garnet (YIG)[2-4, 10, 13-15] which is an incredibly low loss material,[16] but is difficult to fabricate as a thin films as it often requires expensive gadolinium gallium garnet (GGG) substrates.[13, 16] Hexaferrites, such as barium M-type hexaferrite (BaM), have the advantage of uniaxial anisotropy which can reduce the required biasing field in devices, but they are also difficult to fabricate and generally have lower room temperature magnetization and higher coercivity (H_C) than other ferrites.[6, 7, 17-21] Spinel ferrites, such as nickel zinc ferrite (NZFO), are promising for use in integrated microwave devices due to their high tunability, ease of fabrication and relatively improved magnetic properties, such as higher magnetization.[22-25]

The spinel structure consists of a cubic close-packed oxygen lattice with both octahedral and tetrahedral sites occupied by cations. The general formula for these materials is AB_2O_4 where A represents divalent cations and B represents trivalent cations. In spinel ferrites, there are generally two iron atoms per formula unit and the remaining metal cation can be a wide variety of other metals (*e.g.* Co, Ni, Mn, Zn, Cu, Ti, Cr), or any combination of these, which leads to a high degree of tunability. The coupling between spins in adjacent cation sites in spinel ferrites is antiferromagnetic, but often the magnetic moment between the sites is unequal, creating a net magnetization along the direction of the stronger moment. This type of magnetism, termed ferrimagnetism, is thus highly dependent on the distribution of the cations within these sites.[24, 26, 27] This grants spinel ferrites another level of tunability, since the cation distribution is sensitive to the fabrication methods and processing conditions.

Nickel-zinc ferrite (NZFO) is a spinel ferrite that has attracted significant research interest.[26, 28-35] As a bulk powder, it is currently used commercially in a number of discreet microwave components. Due to its high

resistivity and thermal stability, it is often used in devices operating above 5 MHz or at high temperatures.[9] In an effort to integrate NZFO into micro-devices, there have been a number of attempts to fabricate NZFO thin films. The methods employed have included pulsed laser deposition (PLD),[29, 36-39] alternative sputtering,[22, 40] chemical bath deposition,[41, 42] and spin-spray methods.[30, 31, 35, 43] In the cases of PLD and alternative sputtering, the resulting films were found to have high losses,[29, 40] high coercivities,[22, 38-40] or high stress-induced anisotropy fields.[36, 37] The magnetic and high frequency properties of the films made using the chemical bath deposition method were not investigated, however this method yielded films with a flake morphology. While this structure is beneficial for the pseudocapacitive applications they were investigating, these films had a high degree of porosity which often increases losses, making it not an ideal method. Currently, the most promising route to NZFO thin films are spin-spray methods in which a solution of dissolved metal ions or metal-oxide oligomers is sprayed onto a spinning, often heated, substrate. The spin-spray method has a number of advantages including low processing temperatures, a high degree of uniformity in thickness and composition and good scalability. However, NZFO films fabricated using this method often have poor crystallinity which leads to low saturation magnetization (M_S) and, often, a high anisotropy field (H_A).[35]

Here we report a solution-phase, sol-gel based spin-coating route to NZFO thin films with low high-frequency losses, high saturation magnetization and low coercivity. While only spin-coating was investigated here, similar results could be likely be obtained using other related methods, including dip-coating or doctor blading. Solution-phase methods to thin film fabrication are advantageous because they are relatively cheap, scalable and create very compositionally uniform materials. Aqueous solutions have been used extensively as precursors to powders of NZFO and other ferrites as well as being used as the precursor in spin-spray deposition methods,[35, 44-51] but the high surface tension of water makes it less than ideal for many room temperature thin film deposition processes. Indeed, high-quality thin films of a variety of ferrites including pure nickel ferrite have been fabricated using spin-coating and dip-coating methods based on organic solvents containing small amounts of water.[23, 27, 52-55] These organic solvents provide improved the substrate wetting, compared with purely aqueous systems. Here, we utilize a propanol solution of dissolved metal precursors to fabricate NZFO thin films and investigate the effect of annealing conditions and composition on the static and dynamic magnetic properties of the films. We find that films with the optimal composition and annealing conditions have a narrower FMR linewidth than any previously reported NZFO thin films, and a higher saturation magnetization than films prepared using spin-spray methods.

Experimental methods

Materials

Iron (III) nitrate nonahydrate (99.999%) and zinc (II) acetate dihyrdate (97%) were purchased from Alfa Aesar and used without further purification. Nickel(II) acetate tetrahydrate (98%) and 1-propanol (99.7%) were purchase from Sigma-Aldrich and used without further purification.

Preparation of sol-gel precursor solution

The solutions were prepared by dissolving the metal salts in the desired molar ratio into 1-propanol to form a solution with a final concentration of 0.2 M. In a typical synthesis for $Ni_{0.3}Zn_{0.7}Fe_2O_4$, $Fe(NO_3)_3{\cdot}9H_2O$ (0.808 g, 2 mmol), $Zn(OOCCH_3)_2{\cdot}2H_2O$ (0.128 g, 0.7 mmol), and $Ni(OOCCH_3)_2{\cdot}2H_2O$ (0.075 g, 0.3 mmol) were dissolved in 10 mL of 1-propanol. The mixture was magnetically stirred at room temperature for 1 hour at which point the solution was red-orange in color and completely clear. The metal compounds were not dissolved if the solutions were not stirred for more than 30 minutes, and the solutions turned cloudy and unusable after 5 hours.

Film deposition and annealing

The solutions were deposited by spin coating onto clean (100) Si wafers (2 x 2 cm in size) at 2000 RPM for 2 minutes. The film was then immediately heated to 200 ˚C in air for 10 minutes to ensure complete dehydration; this was followed by cooling to room temperature. The films were then crystalized in a quartz tube in a tube furnace under flowing O_2. The temperature was increased to the desired temperature (800-1100 ˚C) at a rate of 20 ˚C/min, and then held at temperature for 30 minutes before the oven was turned off and the films were allowed to cool down slowly.

Characterization

A JEOL JSM-6700F field emission scanning electron microscope (FE-SEM) was used to characterize the microstructure of the films. X-ray diffraction patterns were the result of 2D grazing incidence wide angle X-ray scattering experiments (GIWAXS) performed at the Stanford Synchrotron Radiation Lightsource (SSRL). These experiments were carried out using beamline 11-3, and the resulting 2D diffractograms were integrated to create the 1D patterns presented here. FMR spectra were collected using a Bruker EMX X-band EPR spectrometer operating at 9.72 GHz. The magnetic properties were measured using a Quantum Design MPMS superconducting quantum interference device (SQUID) magnetometer.

Results and discussion

The effect of annealing temperature was investigated on films with a fixed composition of $Ni_{0.3}Zn_{0.7}Fe_2O_4$. **Fig. 1a-d** shows top-view SEM images of the films. The grain size was observed to increase with increased

annealing temperature. XRD analysis performed on the same films **(Fig. 1e)** indicates that the films all have the desired spinel crystal structure with no detectable impurities in films annealed above 900 ˚C. The film annealed at 800 ˚C, however, has an impurity peak at 33.189˚ which corresponds to the (311) peak of Fe_2O_3. The appearance of this phase at temperatures below 900 ˚C is consistent with previous work on ferrite powders.[56]

In order to probe the high frequency properties of these films, X-band (9.72 GHz) FMR was used, and the resulting spectra are presented in **Fig. 1f**. The main Figure of merit we use to evaluate these films is the peak-to-peak linewidth of the FMR spectra, which is a measure of the high frequency magnetic losses. This linewidth can be used to determine the Gilbert damping coefficient, a unitless parameter used to characterize losses in the Landau-Lifshitz-Gilbert (LLG) model,[57] through the following relation:

$$\alpha = \frac{\gamma \Delta H_{\mathrm{pp}}}{4\pi f'} \qquad (1)$$

where γ is the gyromagnetic ratio, which is determined by the FMR resonance field (H_{res}) as discussed below, and f' is the measurement frequency. For most microwave applications, low loss corresponding to low values for α, and therefore low linewidths, are desired. As seen in **Fig. 1f,** the FMR linewidth decreases with increasing annealing temperature from 379 G (α = 0.013) for films annealed at 800 ˚C to 93 G (α = 0.003) for films annealed at 1100 ˚C. All of the linewidths and calculated Gilbert damping coefficients are presented in **Table 1**.

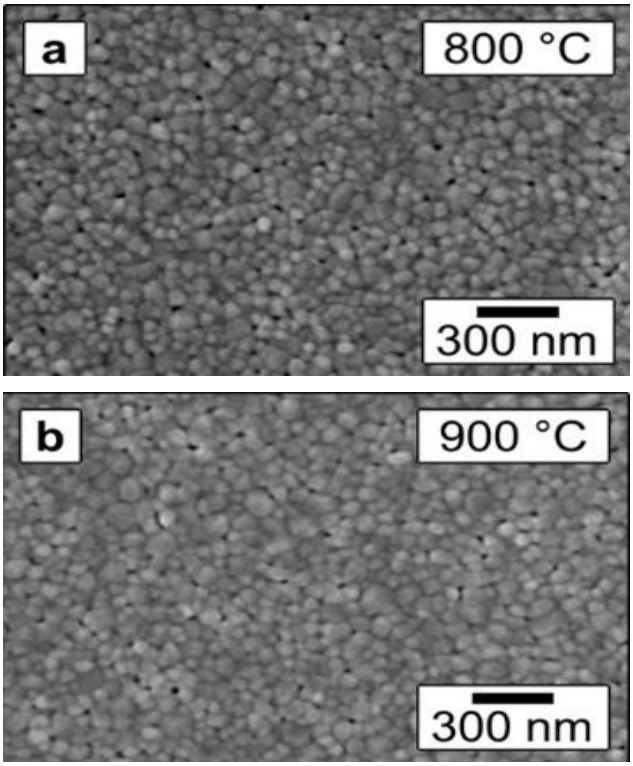

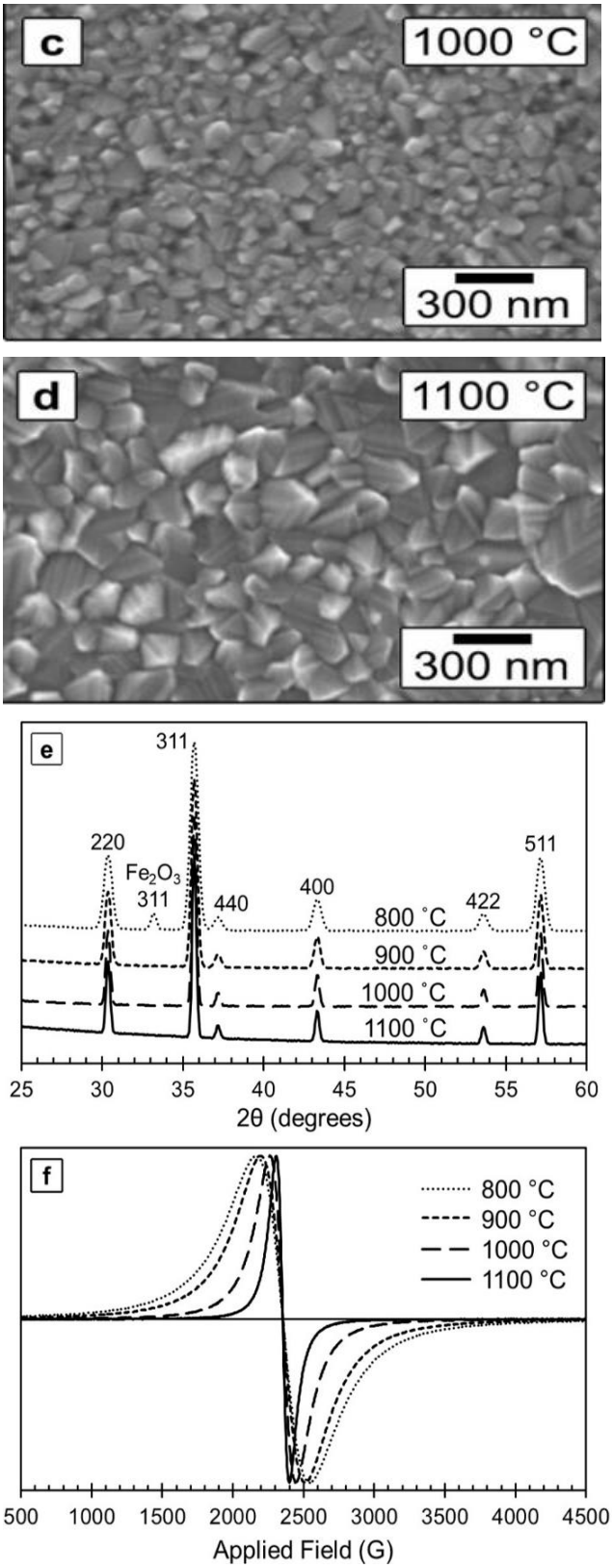

Fig. 1. Top-view SEM micrographs of $Ni_{0.3}Zn_{0.7}Fe_2O_4$ films annealed to (a) 800 ˚C (b) 900 ˚C (c) 1000 ˚C and (d) 1100 ˚C (all images are set to the same scale.) Higher annealing temperatures are seen to increase grain size. (e) X-ray diffractograms of the same films showing the spinel crystal structure for all films with an Fe_2O_3 impurity appearing only in samples annealed to at low temperature (800 ˚C, dotted line). (f) FMR spectra of the same films showing the lowest linewidth for films annealed to 1100 ˚C (solid line).

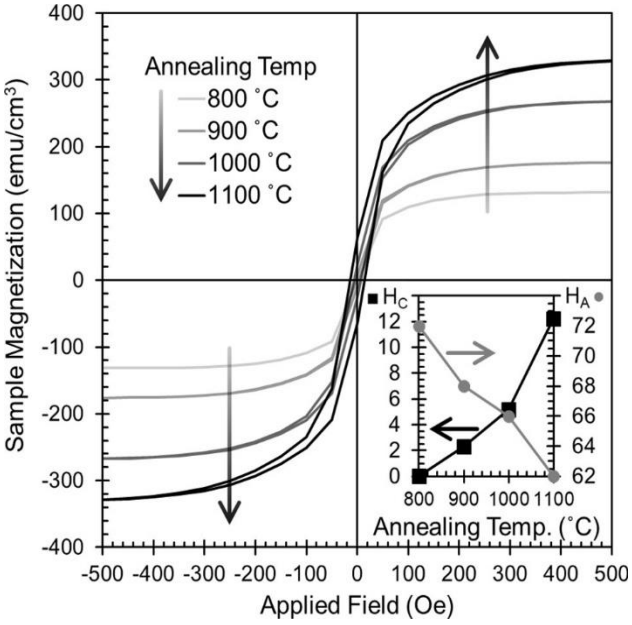

Fig. 2. Room-temperature magnetic hysteresis loops for $Ni_{0.3}Zn_{0.7}Fe_2O_4$ films annealed at various annealing temperatures. (Insert) Coercivity (H_C, black squares) and anisotropy field (H_A, grey circles), determined from the M-H loops as a function of annealing temperature.

The static magnetic properties of these films were investigated using SQUID magnetometry at room temperature, and the resulting M-H loops are presented in **Fig. 2**. The saturation magnetization increases significantly with annealing temperature reaching a maximum of 330 emu/cm^3 for the film annealed at 1100 ˚C. In addition to increasing M_S, the anisotropy field increasing annealing temperature. The H_C and H_A values for the M-H loops in **Fig. 2** are presented graphically in the inset and included in **Table 1**. The film annealed at 1100 ˚C has the lowest anisotropy field (62 Oe), which is desired for most applications, but it also has the highest coercivity (14 Oe), which is not desired for some applications. Despite this fact, from these investigations, we decided that 1100 ˚C was the optimal annealing temperature to fabricate low-loss NZFO films suitable for microwave applications, and thus we used this temperature for the subsequent studies focusing compositional variation, described below.

Table 1. Magnetic Properties of $Ni_{0.3}Zn_{0.7}Fe_2O_4$ Films Annealed to Various Temperatures.

Annealing Temperature (°C)	FMR linewidth (G)	Gilvert Damping Coefficient (α)	Coercivity (Oe)	Saturation Magnetization (emu/cm^3)
800	379	0.013	0	130
900	314	0.011	2	180
1000	183	0.006	5	270
1100	93	0.003	14	330

With the optimal annealing temperature identified, it is interesting to understand why this high temperature is needed. The decrease in FMR linewidth and increase in saturation magnetization with higher annealing temperatures are likely both due to differences in the cation distribution. Previous work has shown that cation distribution plays a large role in determining the magnetic properties of NZFO and analogous systems.[24, 27, 50, 51, 58] Pure $NiFe_2O_4$ is an inverse spinel structure in which the Ni^{2+} cations preferentially occupy octahedral sites while the Fe^{3+} cations occupy the remaining octahedral sites and the tetrahedral sites. However, in $ZnFe_2O_4$, which is a normal spinel, the Zn^{2+} cations preferentially occupy the tetrahedral sites leaving the Fe^{3+} occupying the octahedral sites.[59] When Zn^{2+} cations are substituted into the $NiFe_2O_4$ system, they preferentially occupy tetrahedral sites which forces more Fe^{3+} into octahedral sites. This change in Fe^{3+} cation distribution can have a large effect on the overall magnetic properties.[58, 59]

In the current work, high annealing temperatures can allow for more cation migration during crystallization, while at low annealing temperatures, cation migration is more limited. This likely leads to a more thermo-dynamically-favored cation distributions in films annealed at 1100˚C, and a more kinetically-controlled cation distributions in films annealed at 800˚C. In a kinetically-controlled distribution, the Fe^{3+} cations are more likely to be evenly distributed between octahedral and tetrahedral sites, which would cause those magnetic moments to cancel out, leading to lower saturation magnetization. Furthermore, cation ordering has been shown to effect electrical conductivity in spinel ferrites where the primary conduction mechanism is charge-hoping through percolated networks of redox active Fe sites.[26, 58] Decreased conductivity at higher annealing temperatures[60] likely contributes to the low linewidth observed in films annealed at 1100˚C.

In order to more fully understand the effects of annealing conditions on these NZFO films, we also crystallized films using rapid thermal annealing (RTA). In our standard annealing, as discussed above, the NZFO films are heated in a tube furnace under flowing oxygen for 30 minutes in addition to the time needed for heating up and cooling down. RTA, on the other hand, is able to heat and cool samples in just a few minutes total time. The NZFO films were heated in oxygen to 1080 ˚C over 1 minute and then annealed at that temperature for 1 minute before being quickly cooled to room temperature. Note that 1080˚C was used because it is the highest temperature that our RTA system can achieve. Using this method, we investigated two annealing procedures: films annealed via RTA only, and films pre-annealed at 800 ˚C using our standard annealing procedure, and then RTA annealed to 1080 ˚C.

Top-view SEM images of films annealed using these various methods **(Fig. 3a-c)** show that there is little difference in microstructure for films annealed under different conditions. XRD analysis **(Fig. 3d)**

indicates that films annealed using RTA have the desired spinel structure with same Fe_2O_3 impurity that was previously found in films annealed more slowly at 800 ˚C, which is not desired. FMR investigations found that both films prepared using RTA have significantly larger linewidths than films annealed through our standard method, as shown in **Fig. 3e**. The film pre-annealed at 800 ˚C before RTA treatment (dashed line) has a linewidth of 348 G, which is a small improvement over the film that was only annealed at 800 ˚C using our standard conditions, where the linewidth was 379 G. However, the RTA treatment is unable to remove the Fe_2O_3 impurity, or reduce the linewidth to values comparable to films annealed through the standard method at 1100 ˚C. The film annealed directly to 1080 ˚C using RTA had an even higher linewidth of451 G, suggesting reduced cation ordering, per the discussion above. Thus, slow annealed films like this had more thermodynamic controlled cation distributions, which are favorable for RF applications. In RTA, the short duration of heating leads to a more kinetically-determined cation distribution, which produced materials with relatively high losses.

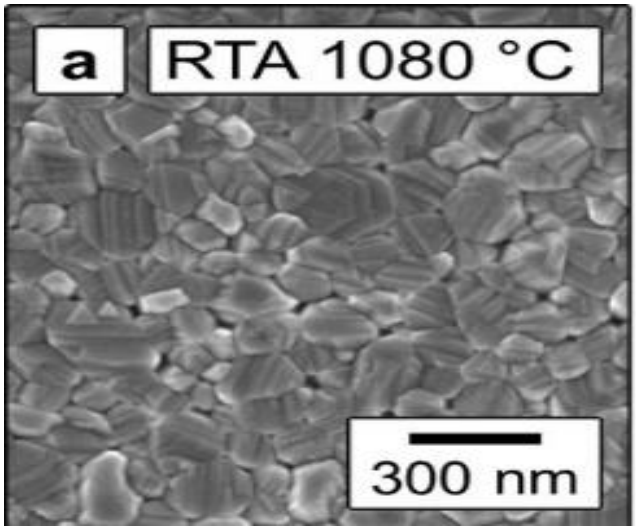

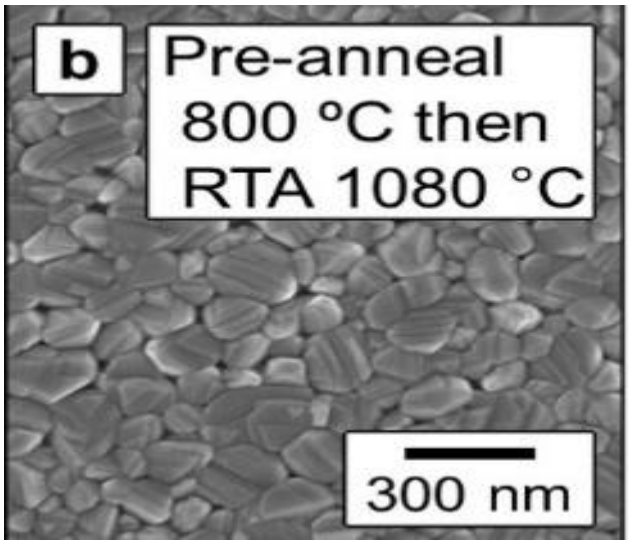

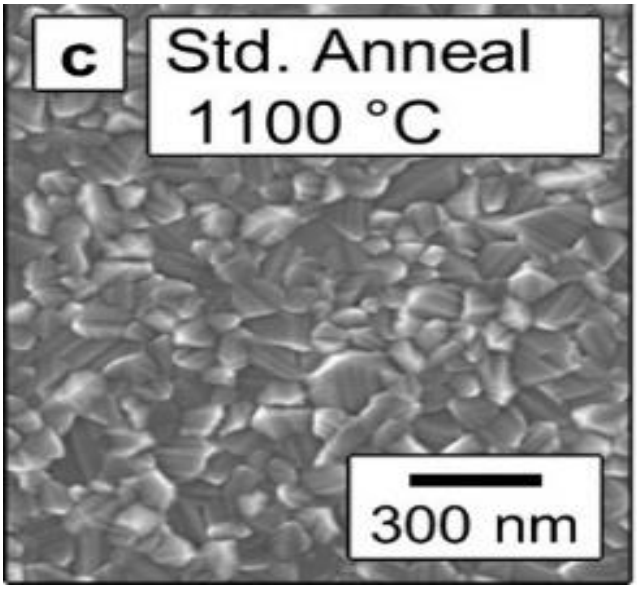

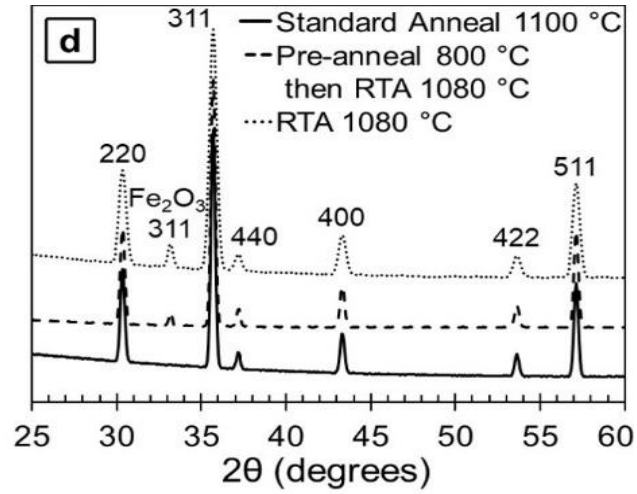

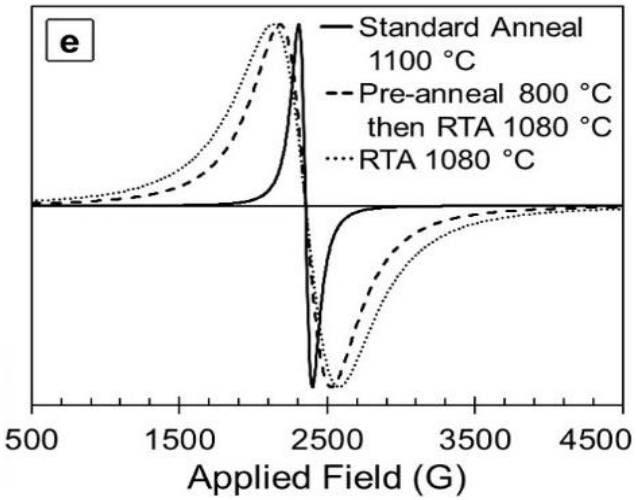

Fig. 3. Top-view SEM images of films annealed (a) using rapid thermal annealing (RTA) at 1080 ˚C, (b) using a standard tube furnace to slowly anneal the sample at 800 ˚C, followed by RTA at 1080 ˚C and (c) using our standard slow procedure in a tube furnace at 1080 ˚C. (d) XRD diffraction powder patterns for the same films showing an iron oxide impurity in both RTA processed films. (e) FMR spectra showing increased linewidths in RTA films compared to films annealed for longer times at 1100 ˚C.

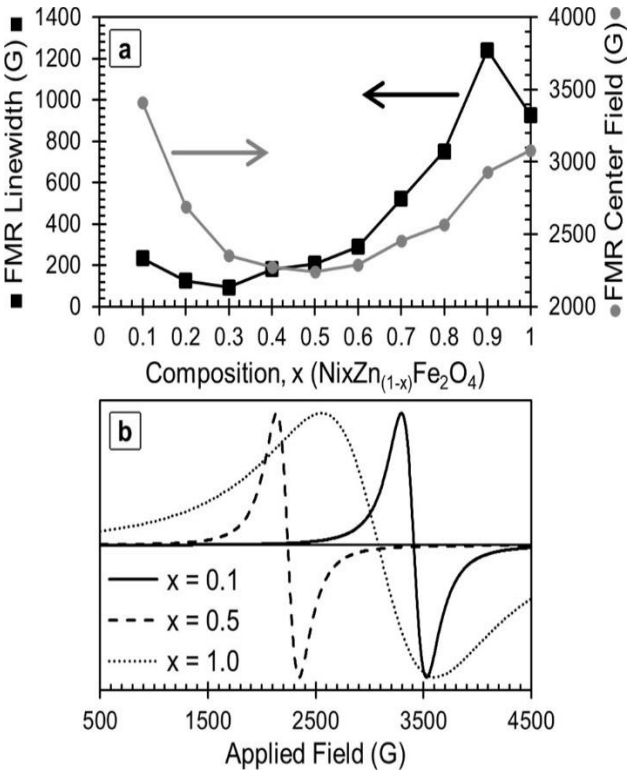

Fig. 4. (a) FMR linewidth (black, left axis) and centerfield (grey, right axis) as a function of composition in $Ni_xZn_{(1-x)}Fe_2O_4$ films. (b) FMR spectra for films with x = 0.1 (solid line), x = 0.5 (dashed line) and x = 1.0 (dotted line).

After determining that slow anneal at 1100 ˚C is the optimal annealing procedure for these films, we investigated the effect of composition. To do this, the ratio of nickel and zinc was systematically changed while the amount of iron was held constant. **Fig. 4a** shows the FMR linewidth (black squares) and center field (grey circles) as a function of composition. Example spectra for samples of $Ni_xZn_{(1-x)}Fe_2O_4$ where x = 0.1, 0.5 and 1.0 are presented in **Fig. 4b**. Lower nickel content samples have generally lower linewidths with the minimum linewidth of 93 Oe being at x = 0.3, $Ni_{0.3}Zn_{0.7}Fe_2O_4$. The FMR center field, or the field at which the intensity reaches 0 between the peaks, reaches a minimum at x = 0.5 **(Fig. 4b, dotted line).** The center field is a material dependent property and thus the change with composition is expected. This value is used in combination with the measurement frequency to determine the gyromagnetic ratio (γ):

$$\gamma = \frac{f'}{H_{\text{res}}} \qquad (2)$$

where f' is the measurement frequency. In addition to being used in calculating the Gilbert damping coefficient (eq. 1), the gyromagnetic ratio is used to determine a device's operation frequency and biasing field.

The room temperature coercivity, anisotropy field and saturation magnetization as a function of composition are presented in **Fig. 5.** The coercivity **(Fig. 5a, black squares)** is generally lower for films with nickel content less than x = 0.4, reaching a minimum of 10 Oe for x = 0.1. H_C reaches a maximum value of 50 Oe at x = 0.7 and then decreases as nickel content further increases. On the other hand, H_A **(Fig. 5a, black squares)** again starts low values of x < 0.4, but H_A then monotonically increases with increasing nickel content up to x = 1.0. The M_S **(Fig. 5b)** lowly increases with increasing nickel content until it reaches a maximum at x = 0.6 and then it decreases more rapidly as nickel content further increases. From this data, low nickel content films are the most promising for most microwave applications where low H_C and low H_A are important. Since high M_S is also desirable, the higher end of that low nickel range becomes preferable. Taking into account the FMR properties of these films, $Ni_{0.3}Zn_{0.7}Fe_2O_4$ is found in this work to be the optimal composition for these thin films.

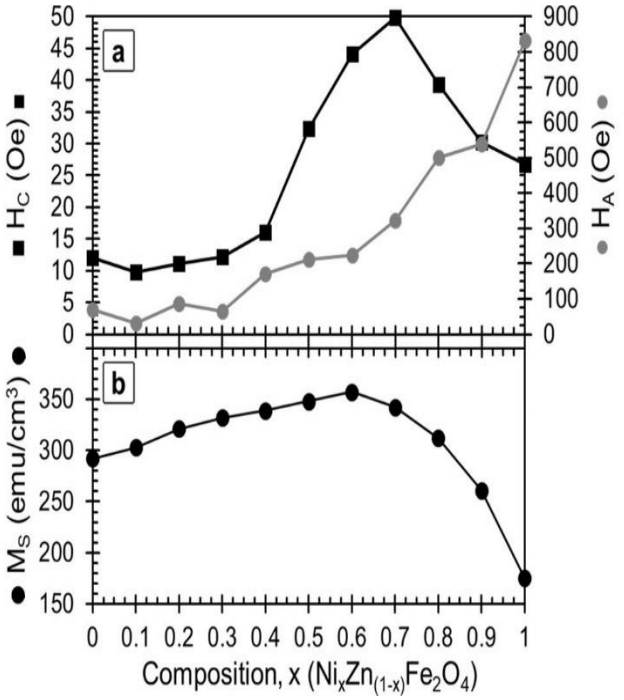

Fig. 5. (a) Room-temperature coercivity (black, left axis) and anisotropy field (grey, right axis) as a function of Ni content. (b) Room-temperature saturation magnetization as a function of Ni content.

Conclusions

Here we present the synthesis of high-quality, low-loss NZFO thin films using a sol-gel method. We found that slow annealing in a standard furnace under flowing oxygen at 1100 ˚C yielded films with the lowest FMR linewidths and highest saturation magnetization. Investigations into the effect of composition suggest that $Ni_{0.3}Zn_{0.7}Fe_2O_4$ is the optimal composition for microwave applications. Films with the optimal composition and annealing conditions were found to have a low coercivity (14 Oe), low saturation field (62 Oe), high saturation magnetization (330 emu/cm^3) and a low FMR linewidth (93 G at 9.72 GHz).

Acknowledgments

This work was supported by the NSF under Cooperative Agreement Award EEC-1160504 as part of the center for Translational Applications of Nanoscale Multiferroic Systems (TANMS). The X-ray diffraction studies presented in this manuscript were carried out at the Stanford Synchrotron Radiation Lightsource. Use of the Stanford Synchrotron Radiation Lightsource, SLAC National Accelerator Laboratory, is supported by the U.S. Department of Energy, Office of Science, Office of Basic Energy Sciences, under Contract DE-AC02-76SF00515. The authors would like to thank Hyeyeon Kang and Patrick Yee for their help in collecting the x-ray diffraction data as well as Abraham Buditama for assistance with rapid thermal annealing of the films.

References

1. G. Srinivasan, I. V. Zavislyak, M. Popov, G. Sreenivasulu and Y. K. Fetisov, *Journal of the Japan Society of Powder and Powder Metallurgy*, 2014, **61**, S25-S29.
2. J. D. Adam, S. V. Krishnaswamy, S. H. Talisa and K. C. Yoo, *Journal of Magnetism and Magnetic Materials*, 1990, **83**, 419-424.
3. X. Y. Sun, Q. Du, T. Goto, M. C. Onbasli, D. H. Kim, N. M. Aimon, J. Hu and C. A. Ross, *ACS Photonics*, 2015, **2**, 856-863.
4. X. Yang, J. Wu, Y. Gao, T. Nan, Z. Zhou, S. Beguhn, M. Liu and N. X. Sun, *IEEE Transactions on Magnetics*, 2013, **49**, 3882-3885.
5. M. A. Popov, I. V. Zavislyak, D. V. B. Murthy and G. Srinivasan, *Microwave and Optical Technology Letters*, 2014, **56**, 814-818.
6. V. G. Harris, A. Geiler, Y. Chen, S. D. Yoon, M. Wu, A. Yang, Z. Chen, P. He, P. V. Parimi, X. Zuo, C. E. Patton, M. Abe, O. Acher and C. Vittoria, *Journal of Magnetism and Magnetic Materials*, 2009, **321**, 2035-2047.
7. Ü. Özgür, Y. Alivov and H. Morkoç, *J Mater Sci: Mater Electron*, 2009, **20**, 789-834.
8. M. A. Popov, D. V. B. Murthy, I. V. Zavislyak and G. Srinivasan, *Journal*, 2012, **48**, 98-99.
9. A. R. Bueno, M. L. Gregori and M. C. S. Nóbrega, *Journal of Magnetism and Magnetic Materials*, 2008, **320**, 864-870.
10. G. M. Yang, J. Wu, J. Lou, M. Liu and N. X. Sun, *IEEE Transactions on Magnetics*, 2013, **49**, 5063-5068.
11. S. Beguhn, X. Yang and N. X. Sun, *Journal of Applied Physics*, 2014, **115**, 17E503.
12. E. Schloemann, *Journal of Magnetism and Magnetic Materials*, 2000, **209**, 15-20.
13. A. Kehlberger, K. Richter, M. C. Onbasli, G. Jakob, D. H. Kim, T. Goto, C. A. Ross, G. Götz, G. Reiss, T. Kuschel and M. Kläui, *Physical Review Applied*, 2015, **4**, 014008.
14. M. C. Onbasli, T. Goto, X. Sun, N. Huynh and C. A. Ross, *Optics Express*, 2014, **22**, 25183-25192.
15. R. Peña-Garcia, A. Delgado, Y. Guerra and E. Padrón- Hernández, *Materials Letters*, 2015, **161**, 384-386.
16. T. Liu, H. Chang, V. Vlaminck, Y. Sun, M. Kabatek, A. Hoffmann, L. Deng and M. Wu, *Journal of Applied Physics*, 2014, **115**, 17A501.
17. R. S. Meena, S. Bhattachrya and R. Chatterjee, *Journal of Magnetism and Magnetic Materials*, 2010, **322**, 2908-2914.
18. Z. Su, Y. Chen, B. Hu, A. S. Sokolov, S. Bennett, L. Burns, X. Xing and V. G. Harris, *Journal of Applied Physics*, 2013, **113**, 17B305.
19. A. Ghasemi, A. Hossienpour, A. Morisako, A. Saatchi and M. Salehi, *Journal of Magnetism and Magnetic Materials*, 2006, **302**, 429-435.
20. H. Sözeri, H. Deligöz, H. Kavas and A. Baykal, *Ceramics International*, 2014, **40**, 8645-8657.
21. G. Tan and X. Chen, *Journal of Magnetism and Magnetic Materials*, 2013, **327**, 87-90.
22. J. Gao, Y. Cui and Z. Yang, *Materials Science and Engineering: B*, 2004, **110**, 111-114.
23. D. M. Schleich and Y. Zhang, *Materials Research Bulletin*, 1995, **30**, 447-452.
24. T.-J. Park, S. Sambasivan, D. A. Fischer, W.-S. Yoon, J. A. Misewich and S. S. Wong, *The Journal of Physical Chemistry C*, 2008, **112**, 10359-10369.
25. L. Ming, Z. Ziyao, L. Ming, L. Jing, D. E. Oates, G. F. Dionne, L. W. Ming and X. S. Nian, *Journal of Physics D: Applied Physics*, 2013, **46**, 275001.
26. M. Atif, M. Nadeem, R. Grössinger and R. S. Turtelli, *Journal of Alloys and Compounds*, 2011, **509**, 5720-5724.
27. S. Seifikar, T. Rawdanowicz, W. Straka, C. Quintero, N. Bassiri-Gharb and J. Schwartz, *Journal of Magnetism and Magnetic Materials*, 2014, **361**, 255-261.
28. U. S. Alaan, G. Sreenivasulu, K. M. Yu, C. Jenkins, P. Shafer, E. Arenholz, G. Srinivasan and Y. Suzuki, *Journal of Magnetism and Magnetic Materials*, 2016, **405**, 129-136.
29. R. Debangsu, S. Sakshath, S. Geetanjali, J. Rajeev, S. V. Bhat and P. S. A. Kumar, *Journal of Physics D: Applied Physics*, 2015, **48**, 125004.
30. S. S. Kumbhar, M. A. Mahadik, V. S. Mohite, Y. M. Hunge, K. Y. Rajpure and C. H. Bhosale, *Materials Research Bulletin*, 2015, **67**, 47-54.
31. X. Wang, Z. Zhou, S. Behugn, M. Liu, H. Lin, X. Yang, Y. Gao, T. Nan, X. Xing, Z. Hu and N. Sun, *J Mater Sci: Mater Electron*, 2014, **26**, 1890-1894.
32. H. Su, H. Zhang, X. Tang, Y. Jing and Z. Zhong, *Journal of Alloys and Compounds*, 2009, **481**, 841-844.
33. A. Verma, M. I. Alam, R. Chatterjee, T. C. Goel and R. G. Mendiratta, *Journal of Magnetism and Magnetic Materials*, 2006, **300**, 500-505.
34. H. Montiel, G. Alvarez, M. P. Gutiérrez, R. Zamorano and R. Valenzuela, *Journal of Alloys and Compounds*, 2004, **369**, 141-143.
35. A. Takayama, M. Okuya and S. Kaneko, *Solid State Ionics*, 2004, **172**, 257-260.
36. P. C. Dorsey, B. J. Rappoli, K. S. Grabowski, P. Lubitz, D. B. Chrisey and J. S. Horwitz, *Journal of Applied Physics*, 1997, **81**, 6884-6891.
37. D. Ravinder, K. Vijay Kumar and A. V. Ramana Reddy, *Materials Letters*, 2003, **57**, 4162-4164.
38. R. G. Welch, J. Neamtu, M. S. Rogalski and S. B. Palmer, *Solid State Communications*, 1996, **97**, 355-359.
39. M. M. Amado, M. S. Rogalski, L. Guimarães, J. B. Sousa, I. Bibicu, R. G. Welch and S. B. Palmer, *Journal of Applied Physics*, 1998, **83**, 6852-6854.
40. M. Desai, S. Prasad, N. Venkataramani, I. Samajdar, A. K. Nigam, N. Keller, R. Krishnan, E. M. Baggio-Saitovitch, B. R. Pujada and A. Rossi, *Journal of Applied Physics*, 2002, **91**, 7592-7594.
41. D. K. Pawar, S. M. Pawar, P. S. Patil and S. S. Kolekar, *Journal of Alloys and Compounds*, 2011, **509**, 3587-3591.
42. D. K. Pawar, J. S. Shaikh, B. S. Pawar, S. M. Pawar, P. S. Patil and S. S. Kolekar, *Journal of Porous Materials*, 2011, **19**, 649-655.
43. A. Masanori and T. Yutaka, *Japanese Journal of Applied Physics*, 1983, **22**, L511.
44. R. V. Mangalaraja, S. Ananthakumar, P. Manohar and F. D. Gnanam, *Journal of Magnetism and Magnetic Materials*, 2002, **253**, 56-64.
45. E. E. Sileo, R. Rotelo and S. E. Jacobo, *Physica B: Condensed Matter*, 2002, **320**, 257-260.
46. A. K. Singh, A. Verma, O. P. Thakur, C. Prakash, T. C. Goel and R. G. Mendiratta, *Materials Letters*, 2003, **57**, 1040-1044.
47. A. K. Singh, T. C. Goel and R. G. Mendiratta, *Solid State Communications*, 2003, **125**, 121-125.
48. A.K. Singh, A. K. Singh, T. C. Goel and R. G. Mendiratta, *Journal of Magnetism and Magnetic Materials*, 2004, **281**, 276-280.
49. J. Azadmanjiri, *Materials Chemistry and Physics*, 2008, **109**, 109-112.
50. C. Venkataraju, G. Sathishkumar and K. Sivakumar, *Journal of Magnetism and Magnetic Materials*, 2010, **322**, 230-233.
51. C. Venkataraju, G. Sathishkumar and K. Sivakumar, *Journal of Alloys and Compounds*, 2010, **498**, 203-206.
52. T. E. Quickel, V. H. Le, T. Brezesinski and S. H. Tolbert, *Nano Letters*, 2010, **10**, 2982-2988.
53. F. Cheng, C. Liao, J. Kuang, Z. Xu, C. Yan, L. Chen, H. Zhao and Z. Liu, *Journal of Applied Physics*, 1999, **85**, 2782-2786.
54. S. Seifikar, B. Calandro, E. Deeb, E. Sachet, J. Yang, J.-P. Maria, N. Bassiri-Gharb and J. Schwartz, *Journal of Applied Physics*, 2012, **112**, 123910.

55. S. Seifikar, B. Calandro, G. Rasic, E. Deeb, J. Yang, N. Bassiri-Gharb and J. Schwartz, *Journal of the American Ceramic Society*, 2013, **96**, 3050-3053.
56. S. Gubbala, H. Nathani, K. Koizol and R. D. K. Misra, *Physica B: Condensed Matter*, 2004, **348**, 317-328.
57. T. L. Gilbert, *Magnetics, IEEE Transactions on*, 2004, **40**, 3443-3449.
58. S. E. Shirsath, B. G. Toksha, R. H. Kadam, S. M. Patange, D. R. Mane, G. S. Jangam and A. Ghasemi, *Journal of Physics and Chemistry of Solids*, 2010, **71**, 1669-1675.
59. A. L. Tiano, G. C. Papaefthymiou, C. S. Lewis, J. Han, C. Zhang, Q. Li, C. Shi, A. M. M. Abeykoon, S. J. L. Billinge, E. Stach, J. Thomas, K. Guerrero, P. Munayco, J. Munayco, R. B. Scorzelli, P. Burnham, A. J. Viescas and S. S. Wong, *Chemistry of Materials*, 2015, **27**, 3572-3592.
60. A. K. M. A. Hossain, S. T. Mahmud, M. Seki, T. Kawai and H. Tabata, *Journal of Magnetism and Magnetic Materials*, 2007, **312**, 210-219.

